10

Autonomous Underwater Vehicle Propeller Simulation using Computational Fluid Dynamic

Muhamad Husaini[1], Zahurin Samad[2] and Mohd Rizal Arshad[1]
[1]*Underwater Robotic Research Group, School of Electric &Electronic Engineering, Engineering Campus, Universiti Sains Malaysia, Penang*
[2]*School of Mechanical Engineering, Engineering Campus, Universiti Sains Malaysia, Penang*
Malaysia

1. Introduction

Recently AUV development was stressed on improving the operation range and time. To achieve this requirement sufficient energy to propel and operate the device must be taken into consideration. However, the AUV power mainly supply by on board battery (Neocleous, and Schizas, 1999). Thus, the range of operation only depends on how much power it has. There are two options in order to improve the operation time, the first is developing very efficient battery and the second is optimized the AUV system either electrically or mechanically. For the first option, it takes time in order to develop very efficient battery. Then for time being, the second option is always selected by the researcher in order to improve the operation range of the AUV. Takinaci and Atlar, (2002) improved the energy power management in order to optimized the power consumption. Olsen, (2004) develops the optimum design of propeller that has less energy consumption but high thrust. Beside that Husaini, et al. (2009) work on AUV hull design by using numerical method to reduce the drag.

As mentioned by Takekoshi, et al., (2005) AUV speed was affected by resistance force along the body. This resistance was due to drag force. Stanway and Stefanov-Wagner (2006) reported that the thrust produced by the propeller was quadraticly by increasing in propeller speed. This phenomenon can be understood by reviewing lifting line theory in Carlton, (2007). Although the thrust was increase in rotational speed, the torque also shows the same behavior Chen and Shih,(2007). In electrical point of view, this torque represents the shaft torque of the motor. This torque will introduced power output of the motor.

From the theory that explained before, power consumption can be minimized by optimizing the propeller speed during operation. As mentioned in Olsen (2004) the power increases by increasing in speed. This is because to increase the speed of the vehicle more, thrust is needed. To increase the thrust, propeller speed must be increased. Thus, the power increases because the torque will be rise due to increasing in propeller speed. By knowing the power and thrust relationship, the developer is able to design the specific control system algorithm for certain task.

Objective of this study is to analyse the performance of the propeller using finite volume method. By predicting the performance using simulation, the experiment number can be minimized. This will lead to reduction in cost and time of developing control system. In this paper the torque, thrust, and efficiency of the propeller was extracted from the simulation. Further this data can be manipulated by the researcher to develop optimum control system. However, in this paper the result manipulation or relationship mapping for developing control system was not covered.

2. Literature survey

With an increasing demand for optimum propeller designs, propeller behavior becomes even more important. This situation has accelerated researchers desire to understand the behavior of fluid around the propeller during its operation. To do this with low cost and less effort, the computational fluid dynamic (CFD) approach was introduced in propeller modeling. This section will review some of the previous works related to propeller simulation by using CFD. The review will only cover the application of CFD in specific propeller problems, such as; cavitations effect and the unsteady simulation of propeller behavior.

In order to highlight the significance of blade element theory in propeller performance prediction, Benini (2004) made the comparison between combined momentum-blade element theory (CMBET) with the three dimensional Navier-Stokes calculation. The CMBET representation of the propeller model was validated with a four blade Wageningen B series propeller. Fluid flow around the same type of propeller geometry was simulated by using FLUENT 6.2 software. Furthermore, the result of the CMBET and CFD simulations were compared with theoretical explanations. The result showed that CMBET was only true to experimental values if the fluid-flow was in 2D, but for CFD the performance of the propeller can still be predicted, with certain degrees of agreement with the experiment, even though the flow is 3 dimensional.

Rhee and Joshi (2003) conducted a study to validate the flow around a marine propeller using unstructured mesh based on the Navier-Stokes solver. The study was conducted based on the P5168 propeller type with a diameter of 0.402 metres, which were designed at the David Taylor Model Basin. For computational study the propeller blades were simply mounted on an infinitely long constant radius cylinder, which served as the hub. There are two types of computational domains developed, which are; base domain and extended domain. The purpose of these two different domains is to examine the influence of exit boundary distance from the blade. For the baseline domain, the upstream is 0.5D from blade, downstream at 0.72D and the outer boundary is 1.43D. While the extended domain upstream and outer boundary remained unchanged, but the downstream was extended to 2D. To minimize the computational cost, only one blade was simulated with the domain divided into 4 parts of 72 degrees each. To model the turbulent flow, there are two turbulent flows applied in this study, which are k-omega and RTSM. Commercial software Fluent 6.2 was used to solve the Navier-Stokes equation and gambit as mesh generator.

The major problem of the marine propeller study is the cavitation effect, where in conventional modeling, such as momentum theory and blade element theory, this effect was ignored (Wald, 2006). However, Young and Shen (2007) showed that there is some change in the performance of the propeller due to the cavitation effect. Therefore, the modeling of propeller must consider this effect to ensure that the performance of the propeller can be

predicted accurately. CFD can significantly predict the thrust and torque of the propeller under the influence of cavitation. For the steady simulation, the domain geometry was the same as that of Rhee and Joshi (2003) where only one blade was simulated. But for the unsteady domain, a complete propeller was simulated with an infinite cylinder in the middle of the blade to serve as a hub. Two types of propeller were investigated in this study, which were the MP017 and Sien Maru propellers. For both cases, the turbulent model (k omega) was used to model the turbulent flow. The solver was segregated, the pressure velocity coupling was SIMPLE and the descretezation method was QUICK scheme. To solve the problem FLUENT 6.2 software code was implemented.

Besides the propeller itself, the performance of the propeller was also investigated by the presence of the stator. The stator in front of, or at the back of, the propeller will increase the efficiency of the propeller (Kerwin, 2001). The stator will act by cancelling the swirl at the hub, which will increase the torque of the propeller. The study of the propeller stator interaction, using CFD, was presented by (Guo et al., 2004). In their study, 3D incompressible RANS equations were solved on the non-orthogonal multi-blocked grid system to analyze the flow of ducted marine propulsion. 3D incompressible code was validated with a turbine blade, where the experiment result was already available. The time averaged pressure coefficient was compared with the experiment and a fairly good agreement was obtained. After the code validation, the flow field around the single-stage ducted marine propulsion was simulated, followed by the plotting of pressure distributions, streamlines and changes of velocity components. The hydrodynamic coefficients and propulsive efficiency were also obtained. The main contribution of Guo et al. (2004) is that the CFD code can be used to study the behavior of the fluid around the propeller in the presence of other structures.

Ideally, turbulence is the phenomena, where the fluid flow was not following the laminar flow behavior. The study of turbulence started in the 18th century, after Reynolds introduced the study of fluid behavior in a tube channel. Reynolds differentiates between these two types of fluid behavior by using the Reynolds numbers. These numbers actually represent the ratio between inertia and viscous forces. At low Reynolds numbers, the inertia force is smaller than the viscous force. In this case, the disturbances are dissipating and the flow remained laminar. At high Reynolds numbers, the inertia force is sufficiently large to amplify the disturbances, and turbulence occurs.

In the CFD simulation of the propeller, the selection of the turbulent model was crucial in order to get an accurate result of the propeller's behavior. Batten et al. (2008) solved the Navier-Stokes equation for viscous flow around the propeller and used a K epsilon turbulent model to represent turbulence behavior. Later, Celik and Gunner (2007) and Phillips et al. (2009) also used a K epsilon turbulence model to solve the turbulent flow around the propeller. However, Li (2006) applied a K omega to model the turbulence flow. From literature, both of these turbulent models give a good agreement with experiments. The simulations carried out by the researchers above were in both steady and unsteady domains. This shows that the K epsilon and K omega are also available for unsteady simulations. Beside these two turbulent models, Vysohlid and Mahesh (2006 and 2007) was specifically working on unsteady simulation and proved that the Large Eddy Simulation (LES) was also good for modeling the turbulent flow around a propeller.

From the review, the performance of the propeller was studied by the previous researchers by using numerical method. This approach is to ensure the design propeller can give

desired result in real situation (Young and Shen, 2007). Many such as Rhee and Koutsavdis (2005), Vysohlid and Mahesh (2006), Celik and Gunner (2007) and Guo et al. (2009) used finite volume method to simulated the behavior of the propeller in various cases. Li (2006) showed CFD simulation can represent the propeller during it operation with small error compare with experimental result. From the review, the simulation of propeller operation by using CFD will be used in this researched in order to reduce the numbers of experiment. Beside that from the previous work there is only few researchers (Singhal et al., 2002; Phillips et al., 2009) simulated the small scale propeller by using the CFD. Rhee and Joshi (2006), Batten et al. (2008), and Ghassemi and Ghadimi (2008) studied the behavior of the fluid around the propeller.

3. Computational fluid dynamic

Propeller performance in open water was calculated in the design stage. The thrust and torque coefficient will be computed using CFD. Because of difficulty in testing the propeller under axial flow, CFD was used to get the performance of the propeller when the water was moving. However, to confirm that the CFD model is correct, a bollard pull test was run to validate the CFD simulation. Yoger (1999) stated that the efficiency of the propeller varies in different advanced ratios. Although the performance of the propeller was already calculated by using the vortex lattice method, this value is purely theoretical and based on the assumption that the efficiency of the propeller was 98 percent of the actuator disc efficiency. This assumption was not correct for real conditions, where the fluid flow was not necessarily moving straight and hitting the disc surface. Therefore, CFD analysis is required to resolve this problem.

In this study, the speed of the propeller varies from 500 to 1500 rpm. The maximum speed was set at 1500 rpm in order to match the PVL propeller design speed. The advanced ratios, was varied from 0.6 to 1.2. Advanced ratios J_S can be calculated using the equation below:

$$J_S = \frac{V_S}{nD} \tag{1}$$

V_S is the vehicle velocity, n is the rotations per second and D is the propeller's diameter. Thus, in FLUENT the value of inlet velocity must be set based on the vehicle velocity (V_S) that can be calculated using Equation (1). The rotational speed of the propeller was set to 500 rpm, 1000rpm and 1500 rpm.

The simulation process was started by importing the STEP file of the propeller from the CAD to the pre-processor, called Gambit. The two main steps carried out in Gambit were domain and mesh generation. The model was then exported to the solver software; in this study, FLUENT 6.2 was used. FLUENT is a finite volume based software that is commercially available to run numerical simulations. The flow field was predicted by solving the 3D incompressible Navier-Stokes equation. Gambit, Fluent package, turbulence model, solver setup and solution control will be briefly explained in the next section.

3.1 Numerical method

For the simulation, a second-order implicit formulation was chosen for temporal discretization and a central-differencing scheme was chosen for spatial discretization. The

solution for continuity and velocity equations continued until the flow became statistically steady throughout monitoring the torque of the propeller. The computations were carried out using FLUENT 6.2, which is general purpose CFD software. The governing equations are written for mass and momentum conservation, such that;

$$\frac{\partial \rho}{\partial \tau} + \nabla \cdot (\rho \vec{v}) = 0 \tag{2}$$

$$\frac{\partial}{\partial t}(\rho \vec{v}) + \nabla \cdot (\rho \vec{v}\vec{v}) = -\nabla \rho + \nabla \cdot \left(\bar{\bar{\tau}}\right) \tag{3}$$

where $\vec{v}$ is the velocity vector in the Cartesian coordinate system, ρ is the fluid density and $\bar{\bar{\tau}}$ is the stress tensor - given by;

$$\bar{\bar{\tau}} \equiv \mu \left[\left(\nabla \vec{v} + \nabla \vec{v}^T \right) - \frac{2}{3} \nabla \cdot \vec{v} \right] \tag{4}$$

where α is the molecular viscosity and the second term, on the right hand side, is the effect of volume dilation. Once the Reynolds averaging approach for turbulence modeling is applied, the Navier–Stokes equations can be written in Cartesian tensor form as follows;

$$\frac{\partial \rho}{\partial \tau} + \frac{\partial}{\partial x_j}(\rho u_i) = 0 \tag{5}$$

$$\frac{\partial}{\partial t}(\rho u_i) + \frac{\partial}{\partial x_j}(\rho u_i u_j) = -\frac{\partial p}{\partial x_i} + \frac{\partial}{\partial x_j}\left[\mu \left(\frac{\partial u_i}{\partial x_j} + \frac{\partial u_j}{\partial x_i} - \frac{2}{3} \delta_{ij} \frac{\partial u_i}{\partial x_i} \right) \right] + \frac{\partial}{\partial x_j}\left(-\rho \overline{u_i' u_j'} \right) \tag{6}$$

Where δ_{ij} is the Kronecker delta, and $-\rho \overline{u_i' u_j'}$ is the Reynolds stresses. The Reynolds stress term is related to the mean velocity gradients, i.e., turbulence closure, by the Boussinesq hypothesis as;

$$-\rho \overline{u_i' u_j'} = \mu_\tau \left(\frac{\partial u_i}{\partial x_j} + \frac{\partial u_j}{\partial x_i} \right) - \frac{2}{3} \left(\rho k + \mu_\tau \frac{\partial u_i}{\partial x_i} \right) \delta_{ij} \tag{7}$$

The k–omega model is one of the most widely used turbulence models for external aero- and hydrodynamics and has shown a better potential to predict the key features of vertical/ separated flows than other models. In this study, CFD code employs a cell-centred finite-volume method, which allows use of computational elements with arbitrary triangulation shapes. Convection terms are discretized using the second-order accurate upwind scheme, whilst diffusion terms are discretized using the second-order accurate central differencing scheme. It should be noted here that the thrust of the present study is the application of the unstructured dynamic meshing techniques and efforts are being made to enable higher order accurate schemes for dynamic meshing. The velocity–pressure coupling and overall solution procedure is based on a SIMPLE type segregated algorithm, adapted to an unstructured grid. The discretized equations are solved using point-wise Gauss–Seidel iterations, and an algebraic multi-grid method accelerates the solution convergence.

3.2 CFD control data setup

In order to develop the thruster control system for AUV applications, the relationship between the speed of the propeller and the thrust must be determined. Common practice in AUV development is that the control system must be developed in parallel due to time constraints. For this reason, the CFD simulation is required to give the relationship between speed and thrust of the propeller. For this study, the speed of the propeller was varied and the axial flow was set constant. This test is also known as a bollard pull test, where the water is static and the propeller rotates. In addition to studying the relationship between thrust and speed, this experiment importantly validates the CFD simulation.

3.3 Simulation procedure

There are many constraints to consider when completing this simulation. One of them is model development. The model was generated in the pre-processor stage, where the mesh type was selected from either a structured or unstructured mesh. In the case of the propeller, the unstructured mesh must be selected due to the complexity of the geometry. After meshing process, the boundary conditions for each surface must clearly be defined. An accurate setup for boundary conditions is important for any numerical solutions, to ensure the accuracy of the solution. The mesh process was finished with the export of the mesh file into the solver software. The solver should recognize the mesh as being set in the pre-processor software.

The mesh model, generated previously, will be solved by the solver software. Before the solver starts to solve the problem, the quality of the mesh was evaluated. If the mesh quality was poor, then it has to be refined. In the solver, the turbulence model and material properties were selected in order to predict the fluid behavior in the system. After that, the boundary condition values and solution control parameters are specified. Then the problem is ready for initialization step, which will stop when the calculations are computed. Finally, the results of the computation will be analyzed.

3.4 Pre-processing

In the pre-processing stage, the propeller model with a scale of 1:1 was imported into GAMBIT for the meshing process. The propeller model was saved as a para-solid file in SolidWorks to ensure that the propeller profile is maintained when exported into Gambit. Another option was to save as STP, IGES or STL file format. But this option is not suggested because it will lead to some geometry lost. If the file is in IGES, imported files will have numbers on the edge that are not required in the meshing process. This edge finally needs to be reconnected in Gambit. This process consumed unnecessary time for the grid process.

GAMBIT was used as the pre-processor for geometry modeling due to several of its advantages. GAMBIT is very user friendly in terms of generating a mesh. Besides that, this software has broad options for CAD modeling that it accepts. Important considerations when selecting the pre processor software were that the generated mesh file must be accepted by the solver that will be used. GAMBIT has no problems with this issue, because it is easily accepted by many main commercial solvers such as FLUENT, FIDAP, RAMPANT, NEKTON, POLYFLOW and GENERIC.

3.5 Geometry setup

This section presents details of the model geometry development. In real situations, the propeller will operate in water. For the simulation, water was developed and declared as a

domain. Domain size was importantly studied, because it is related to computational accuracy and machine capability. If the domain is too large, the time consumed in calculation is longer, but if the domain is too small, it will not represent real situations of the phenomena. The domain size in this study was referring to (Vysohlid and Mahesh, 2006). The domain was given in terms of propeller diameter.

For the propeller, the mesh must be smaller in comparison to the domains mesh. This step reduces errors of discretization, due to the complexity of the propeller's geometry. Besides that, the fine domain around the propeller can be used to rotate the water whilst the simulation is in process. Referring to Vysohlid and Mahesh (2006) domains, the computation was in a cylindrical form. From the scale that mentioned by Vysohlid and Mahesh (2006), the cylinder with a diameter of 0.5 meters and length 1 meter has been created. And for the smaller domain around the propeller, the diameter was set to 0.15 meters and length was 0.2 meters.

3.6 Grid generation

The computational grid was divided into three parts for this study. The parts were named as; domain, rotation part and propeller geometry. As shown in Figures 1 and 2. To minimize computational time, the numbers of cell must be decreased. To achieve this, the simulation domain must be split into three sub-domains, as shown in Figure 2. The main cylinder was divided into 120 degree sections. Only one blade was considered in this simulation and assumes that the other blade will performed as a key blade. The reason to create a smaller cylinder around the propeller in this study was that the propeller was fixed but the water surrounding it was rotating. Without this small cylinder, the rotation of the water must include all the water inside the domain.

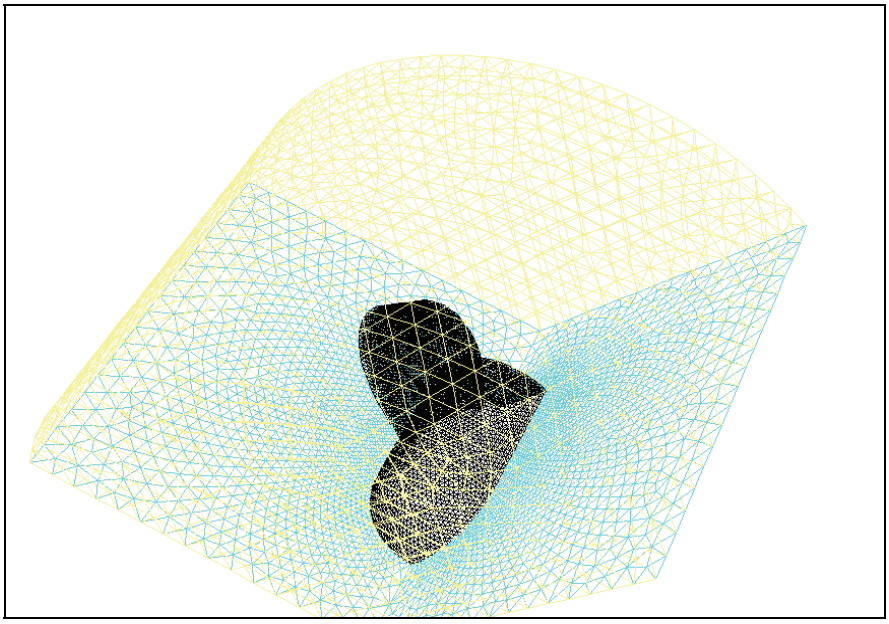

Fig. 1. Rotation part of domain

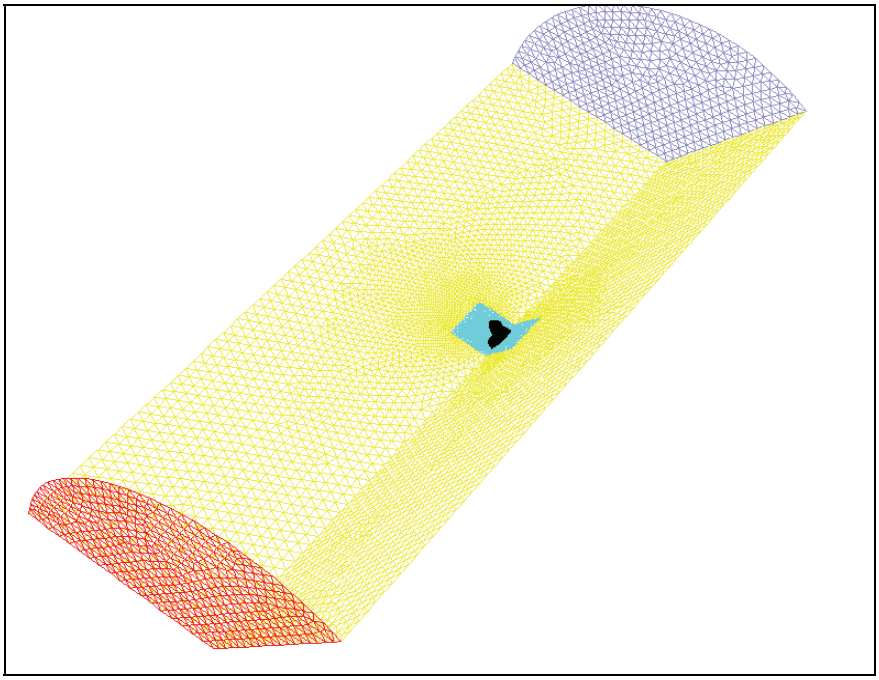

Fig. 2. Computational domain

This is a totally wrong situation, where the water in the far field (main domain) must be moving axially or static, depending on input. Boundary conditions were set to simulate the flow around a rotating propeller in open water: on the inlet boundary, the velocity components of uniform stream with a given inflow speed were imposed; on the exit boundary, the static pressure was set to a constant value - zero in non-cavitating cases, while other variables were extrapolated; on the outer boundary, a slip boundary condition was imposed, i.e., zero normal velocity component with extrapolated tangential velocity components and static pressure; on the blade and the hub surface, the no slip condition was imposed; and on the periodic boundaries, rotational periodicity was ensured.

3.7 Boundary condition

For the validation process, the velocity inlet was set to zero. This condition was chosen to represent the bollard pull condition, where the water is static and the propeller didn't move. After the validation process, the velocity inlet was varied to represent the advanced speed of the underwater vehicle. The variation of the velocity inlet was used to study the performance of the propeller under various vehicle speeds. In this simulation the gauge pressure was set to zero. Back flow direction specification method was set to normal to boundary. To ensure that the water in the pill box domain and the main domain interact, the surface of the pillbox must be set as an interface. The blade surface was set as a non slip wall. Because the domain was divided into 3, the surface must be set symmetrically. This set up can be utilized to avoid redundant calculations in other identical parts.

3.8 Grid dependency study

In the CFD simulation, the grid setup made a big impact to the accuracy of the simulation. Versteeg and Malalasekera (2007) listed three main factors that lead to simulation errors. The three errors that have been listed are; numerical, coding and user errors. Amongst these three errors, the numerical error was directly related to the geometry setup. For numerical errors, three types of error were recognized, namely; round off, iterative convergence and discretization errors. In theory, discretization errors can be minimized by a reduction of the timing step and space mesh size. However, by doing this the computing time and amount of memory required also increased. Here, grid sensitivity takes place to find the optimum setup between memory and computational time against the accuracy of the result.

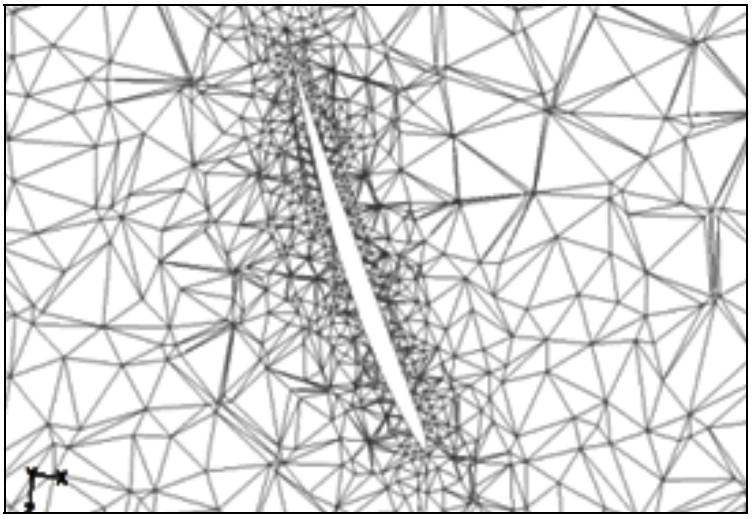

Fig. 3. Coarse meshes surround the blade

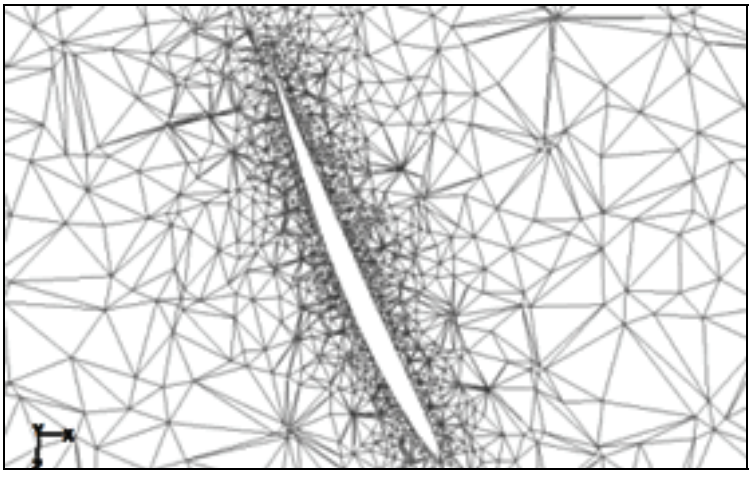

Fig. 4. Medium meshes surround the blade

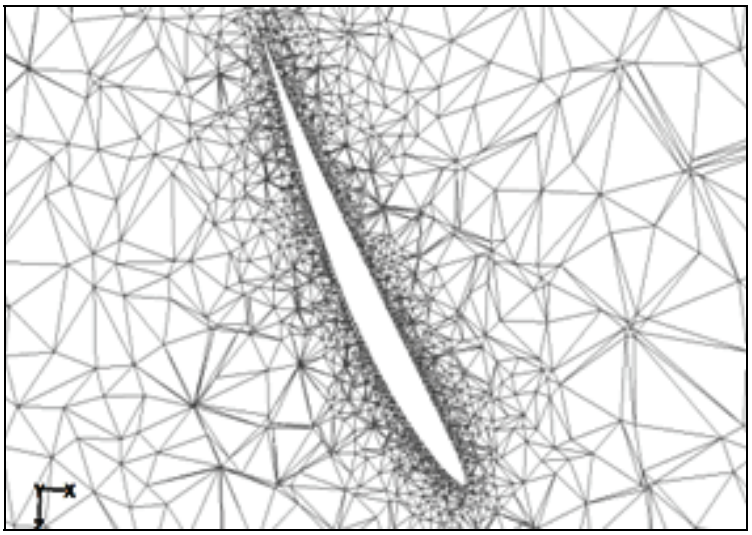

Fig. 5. Fine meshes surround the blade

For the grid sensitivity study, the same domain geometry was kept with three different kinds of mesh. The meshed grids were named as; coarse mesh, medium mesh and fine mesh. For coarse mesh, 154649 numbers of cells were used. For medium mesh, the number of cells was increased 2 times to 378784. Finally, for fine mesh, the number of cells was increased 2 times that of medium mesh, to become 620415. Figures 3, 4 and 5, show different size of meshes around blade boundary.

4. Result and discussion

In the previous section, the performance analysis method of the propeller was shown. However, the experiment run was only in bollard pull conditions. In real applications, the propeller will move together with the vehicle. Due to experimental limitations, CFD was used to study the performance of the propeller by giving an advanced speed. The test results above will be used to validate the CFD simulation.

4.1 Grid Independency

As mentioned in section 3, the model geometry was meshed in three types, namely; fine, medium and coarse mesh. Table 1 shows the simulation results of the four types of mesh. The thrust value of the propeller was taken at 1500 rpm, and the water was static. The results from simulation were compared with the experiments results. The percentage error was calculated with subtract the simulation result from the experiment result then divided with the experiment result. The experiment thrust recorded at this speed was 14.6 Newton.

The simulation results were compared to the experiment result. This comparison was made because in this study, CFD was used as a tool to measure the performance of the propeller in real cases. From the grid dependency study, errors were reduced by increase the numbers of cells. The Table 1 above also shows the simulation errors. By applying the

medium mesh, the errors for the simulation were 5.41%. This error value was considered small, and the CFD result was valid for further analysis. The graph in Figure 6 shows the plot of both the CFD result and the experiment for power input. From the graph, the patterns were similar. This shows that CFD can predict the behavior of the propeller within small errors. However, from the graph, the errors of CFD were increased by the increase in speed. One of the reasons for this limitation is due to the limitation of CFD in predicting turbulent flow. When the rotation of the propeller increased, the Reynolds number also increased. Therefore, the turbulent intensity also increased and the flow became more chaotic and unpredictable.

4.2 Thrust coefficient

The graph in Figure 7 shows the thrust coefficient against advance ratio. These K_t values actually represent the thrust behavior. The trend clearly shows that the K_t values decrease when the advance ratio increases. This phenomenon can be explained by the momentum theory, which was introduced by Rankine in 1865, even though this theory does not consider the geometry of the propeller (Carlton, 2007). In this case, the propeller system can be modeled by this approach, in order to simplify the explanation. In this theory, thrust was calculated by using equation (8) below:

$$T = m\left(v_c - v_a\right) \tag{8}$$

Where, T ,m, v_c and v_a is thrust,mass of fluid, incoming velocity and accelerated velocity. From the equation, it can be seen that the difference in velocity affects thrust generation. Referring back to the graph in Figure 6, the thrust was decreased by increasing in the speed of the axial velocity. This is correct, because at a low axial velocity, the difference of velocity is greater. This occurs because, at this axial velocity, the water surrounding the propeller will be accelerated from a low velocity. At the higher advanced velocity, water surrounds the propeller, which is already moving at a high velocity. Therefore, the propeller makes less change to the water velocity.

Mesh	Predicted thrust (N)	Cell numbers	Percentage error
Coarse	11.3974	154649	21.93%
Medium	13.81	378784	5.41%
Fine	14.12	620415	3.28%

Table 1. Grid dependency study results

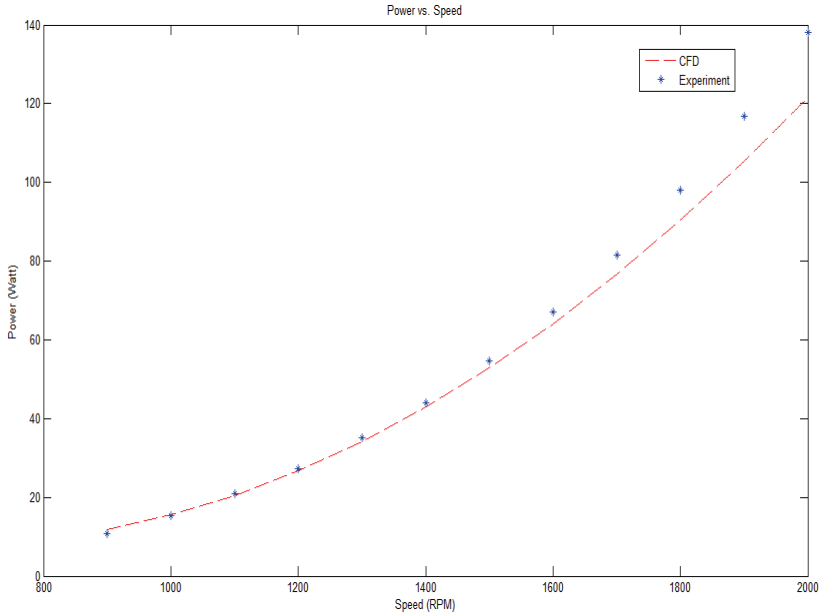

Fig. 6. Plot of power input against propeller speed

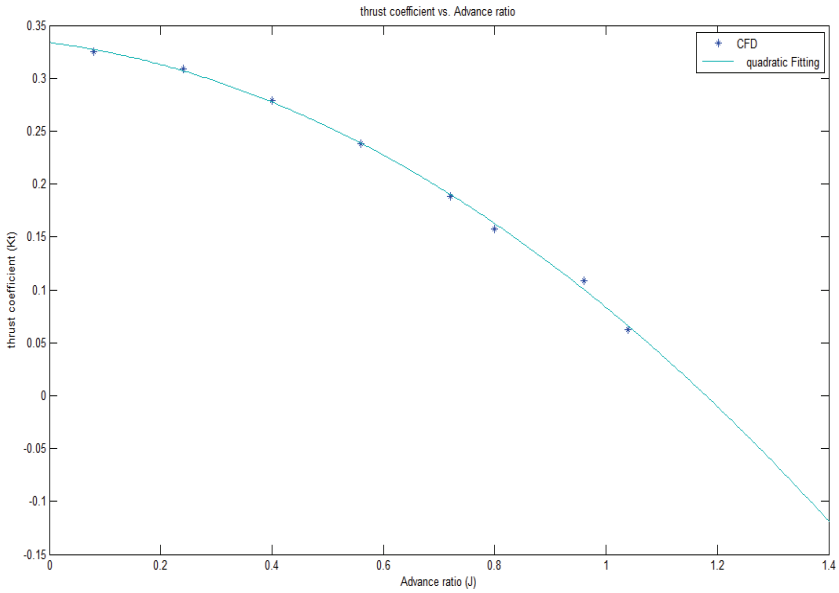

Fig. 7. Plot of Thrust co-efficient against advanced ratio

4.3 Torque coefficient

The graph in Figure 8 shows the relationship between Torque coefficients and advanced ratios. The trend of this graph is similar to the thrust coefficient against advance ratio. This graph shows the behavior of propeller torque under different advanced ratios. From the graph, it can be seen that the torque decreases by increasing the advance ratio. This phenomenon occurs due to a decreasing drag force on the blade surfaces. According to aerofoil theory the propeller torque is calculated by a summation of all drag forces along the blades surface (Wald, 2006).

When the water is almost static, or at a low velocity, the propeller consumed more torque in order to accelerate the water. This is because, at the low speed, the water pressure surrounding the blade was high, which contributes as pressure drag on the blade surface. However, when the water started moving with a higher velocity, this pressure will drop slowly and subsequently, the pressure drag also drops. Compared to viscous drag, pressure drag gives a more significant value to the propellers overall drag. Therefore, by increasing the advance ratio, the torque of the propeller will reduce, as the pressure drag affecting the blade surface drops.

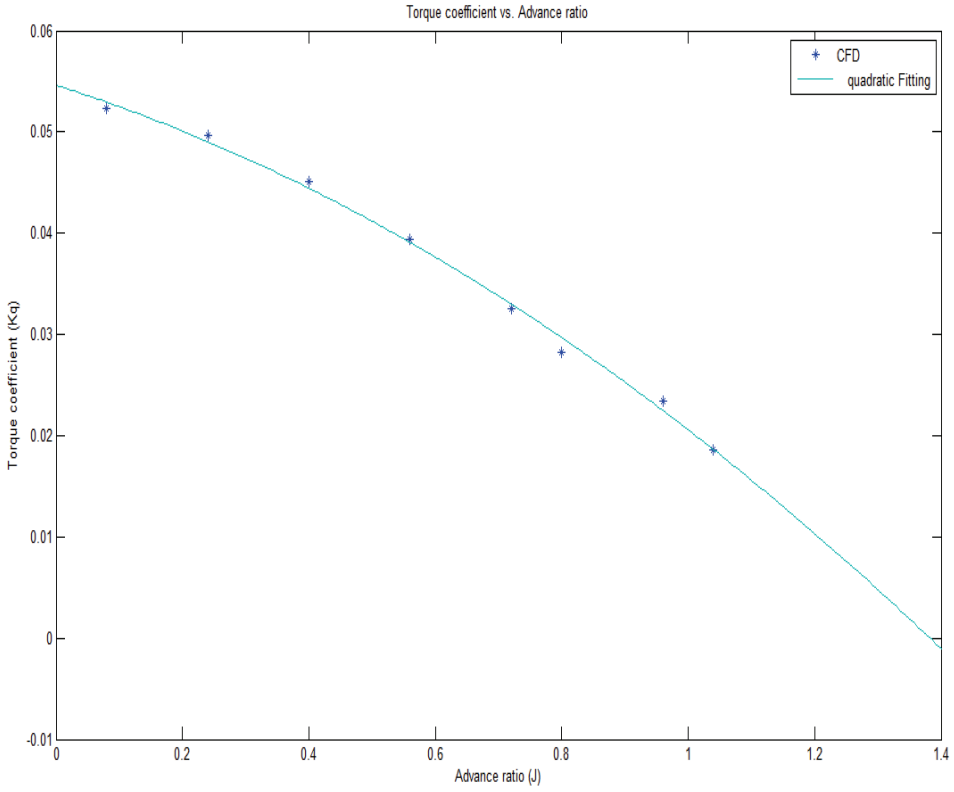

Fig. 8. Plot of torque coefficient vs. advance ratio

4.4 Efficiency vs. advanced speed

The graph in Figure 9 shows the plot of efficiency against advance coefficient. From the graph, it is clear that the peak occurs at efficiency equal to 64.54 %. At this efficiency the advance coefficient was 0.85. During the design stage, the highest propeller efficiency was predicted to occur at an advance ratio equal to 0.8. This shows that the highest efficiency occurred at a different advance coefficient. The trend of the graph was close to the experiment shown by (Lin et al., 2009). However, the efficiency value was different to the design value within a 14 % margin. This error was due to the geometry of the propeller that was used in the simulation. Besides that, the predicted efficiency during the design process was a theoretical value only.

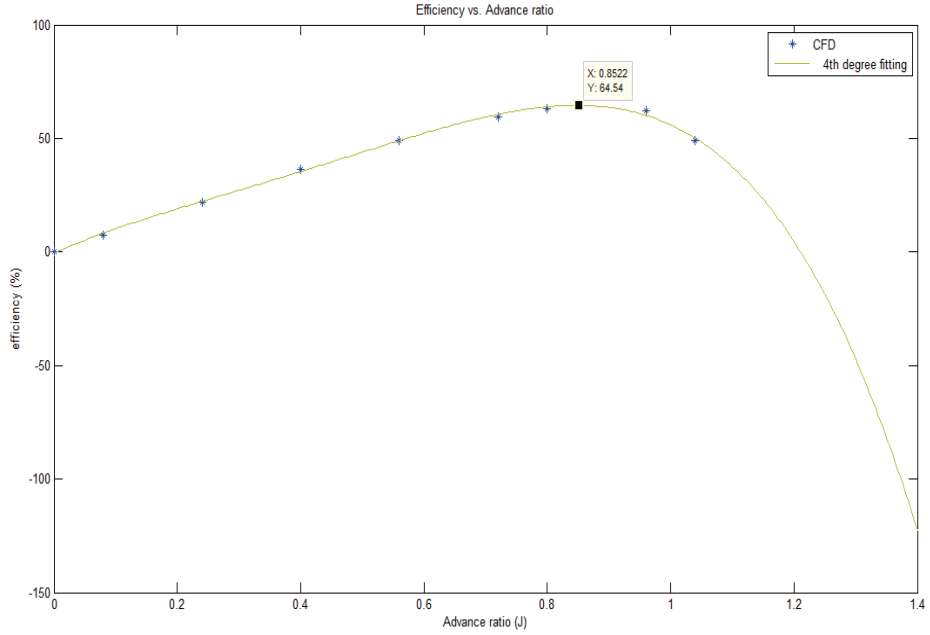

Fig. 9. Plot of efficiency vs. advance ratio

During the design stage, the hub effect was not considered, and the geometry did not have any changes. Nevertheless, in real applications, in order to suit the manufacturing process, the geometry must have a few changes. The CFD simulation utilized the geometry that contained some modification. Another factor of this error was that the theoretical calculations used in design process, contained a few assumption, such as no tangential velocity hitting the blade. The axial velocity was also assumed constant along the blades span. However, in real conditions, even small portions of tangential velocity will affect propeller performance. In the CFD, this tangential velocity was considered by solving the Navier-Stokes equation, where all fluid directions were taken into account. Additionally, the axial flows hitting the propeller are not constant along the blade span. There is always a variation of axial velocity along the blade span starting from the hub up to the blade tip. This variation was due to hub effect and reverse flow during the propellers operation. Some

of the water will be circulated back to the blade surface and then this type of flow will perturb the incoming water flow. Therefore, the axial inflow will be changing according to the perturbation.

In the CFD simulation, this water stream can be modeled with a high accuracy and the effect of this circulation can then be simulated. To fill the fabrication requirement, the tip of the blade must be cut off by 5%. This small change will affect the efficiency of the propeller. During the design process, the geometry was considered completely from the hub to the tip. Nevertheless, following the modification mentioned before, the geometry will be different. A CFD simulation used this geometry to obtain the real performance of the propeller. In Section 4.1, the CFD simulation showed a good agreement with the experiment results. This phenomenon occurred because in the CFD simulation the geometry and the operating conditions followed the experiments conditions. In this case, the CFD results can be used to predict the real performance of the propeller. The error between the design and the CFD simulation can be ignored because the goal of this research is to predict real performance of the propeller after fabrication by way of the cold forging process.

4.5 Fluid behavior surrounding the blade

Figures 10 and 11 show the velocity of the water around the blade at 0.7 radius. The propeller rotation was at 1500 rpm. In Figure 10, the water velocity was zero and in Figure 11 the water velocity was 2 m/s. In the bollard pull condition, the contour difference was evident, because the fluid was starting to move upwards from zero. However, for the advance coefficient 0.8, the velocity contour surrounding the blade showed no significant difference.

This behavior was due to the initial speed of the fluid, which was set at 2 m/s. Therefore, the fluid hitting the blade surface had initial speed and was not constant. Subsequently, the fluid direction, when it hits the surface, was normal to the surface. In the bollard pull condition, the water contour close to the blade also had a certain speed. This pattern of contour showed that the water was moving towards the propeller. Then this water is accelerated by the propeller in a backwards direction. This condition makes different velocities occur at the front and the backside of the propeller blade. The same phenomenon also occurred for fluid that had advance coefficient 0.8.

According to the Bernoulli principle, when the velocity is high, then the pressure will drop, and vice versa. As a result, the pressure surrounding the blade will be different between the back and front sides, as shown in Figures 12 and 13. This difference in pressure will create force on the blade, based on Pascal's rule, where the force is equal to pressure over an area. Because the pressure on the front side was higher than backside, the resulting force will push the propeller in one direction.

However, in Figures 12 and 13 the pressure contour between the two conditions has different patterns. In the bollard pull condition, the high-pressure contour was clearly seen, but in the advance coefficient condition, the lower pressure contour was clearer compared to high pressure. This pattern occurred because in the advance coefficient condition the water velocity hitting the blade surface was higher. Most of the water velocities are identical when they hit the blade surface. Therefore, the velocity contour for this area will have the same colour. For bollard pull conditions, the pressure contour was clear, because during this condition, the pressure behind the blade had an identical value along the blade. This is because the velocity of the water was only affected by the rotation of the blade. Besides that,

in advance coefficient conditions, the water that had velocity, will drag the water behind the propeller and move together. These circumstances make the velocity of the water behind the propeller increase and well distributed.

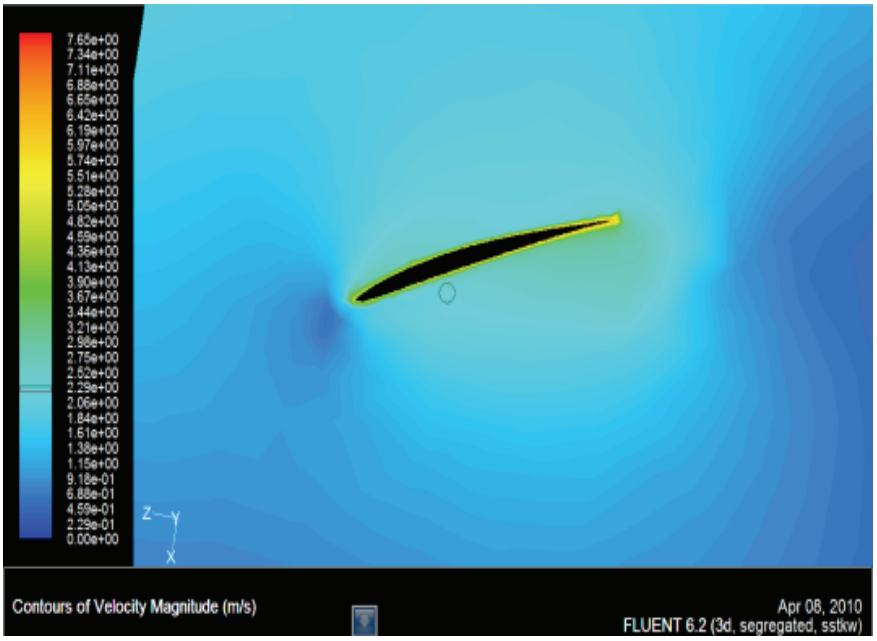

Fig. 10. Velocity contour surrounding the blade at 1500 rpm and bollard pull

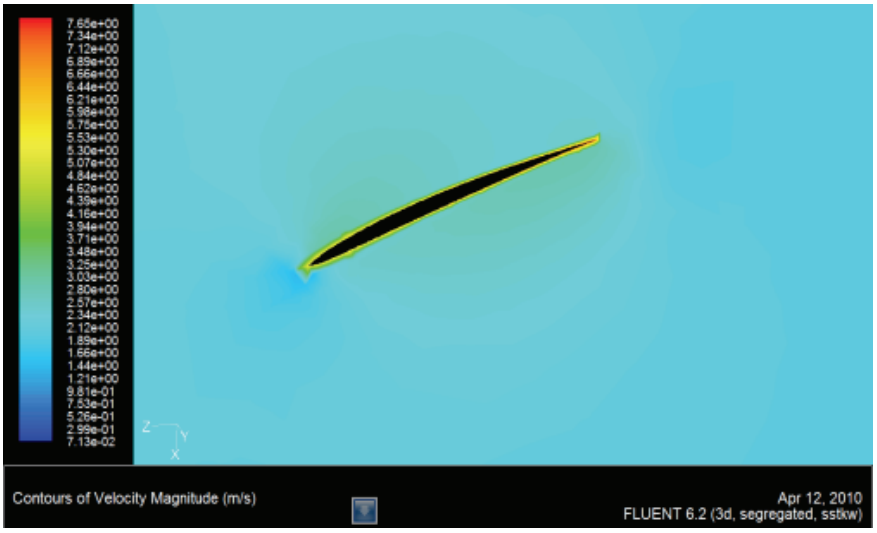

Fig. 11. Velocity contour surrounding the blade at 1500 rpm and 0.8 adv

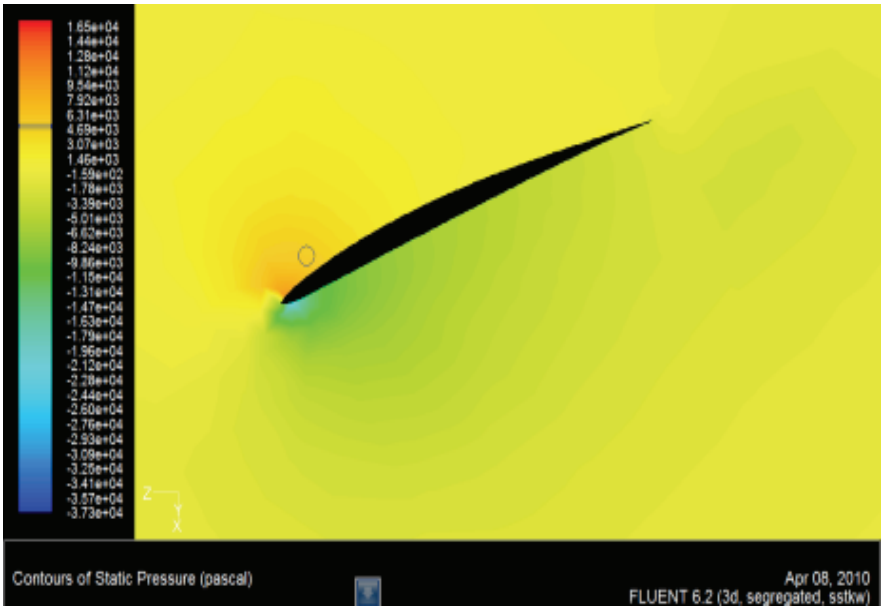

Fig. 12. Pressure contour surrounding the blade in bollard pull condition

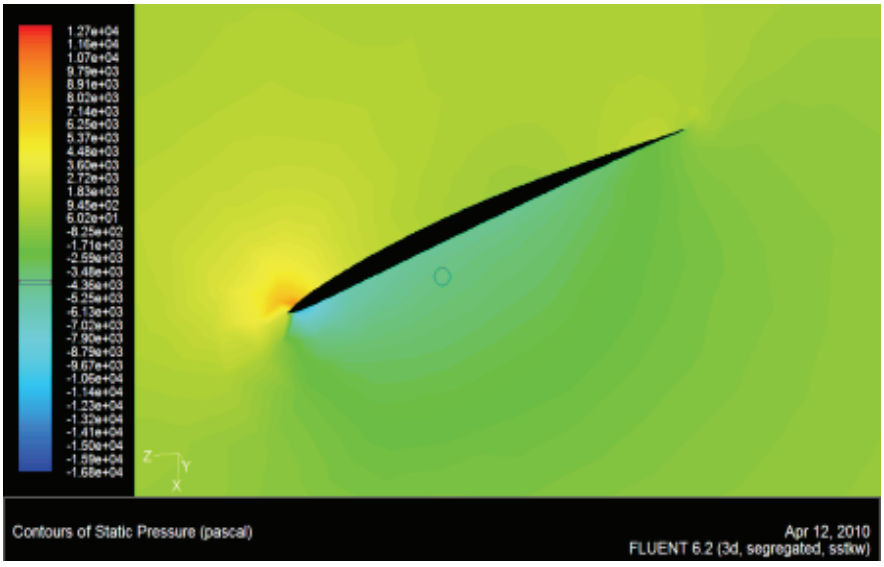

Fig. 13. Pressure contour surrounding the blade at 0.8 adv

4.6 Pressure coefficient distribution along the blade at 0.8

Figures 14 and 15 show the pressure distribution along the blade. The result of this simulation was important in order to know the actions of pressure along the blade surface.

In the figures above, pressure was concentrated at the leading edge. This was also true for the backside of the propeller blade, with the lowest pressure occurring at the leading edge. The higher pressures occur at the 0.9 radius of propeller. This is because, at this radius, the

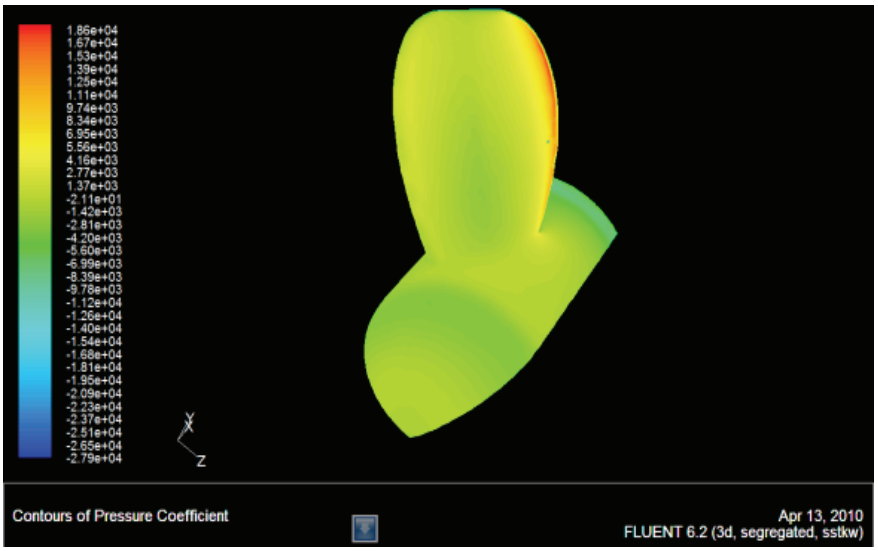

Fig. 14. Pressure coefficients on the back surface

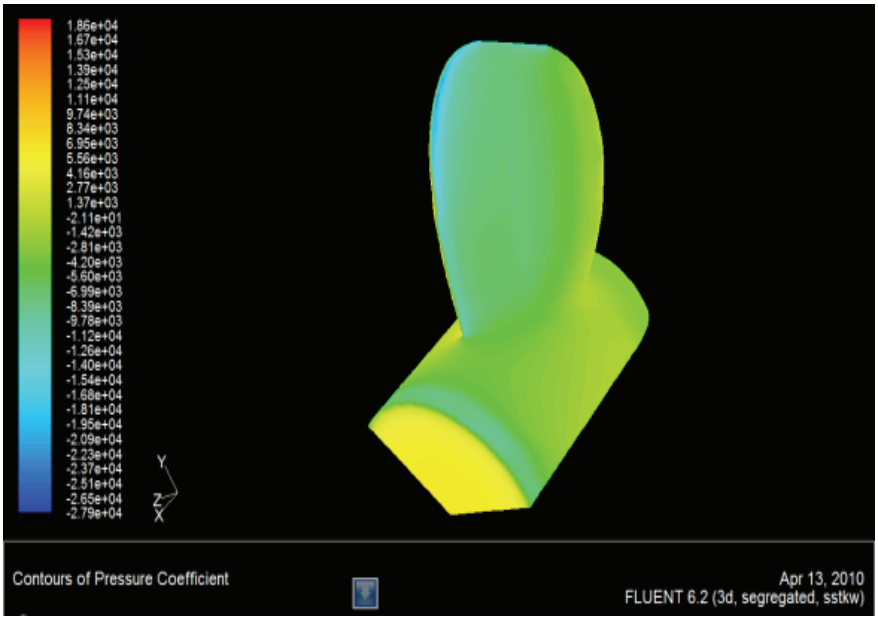

Fig. 15. Pressure coefficients at the front surface

chord length was higher compared to other radii. When the chord length higher, the water will hit this part first, before hitting other parts. The interaction between the blade and the water makes the fluid flow changing in direction and velocity. At the first interaction, water flow will separate into two directions. One will move through to the backside and another will move through to the front side. At radius 0.7 the water velocity will drop suddenly at the front side and increase at the backside. Then the water will face other parts of the propeller blade. At this stage, the water changing direction will already be absorbed by other parts of the propeller. This is the reason why, at the highest chord length, the pressure at the backside is higher and at the front side, it is lower.

From Figure 14 and 15, the force pattern along the blade can be measured. This behavior is important, because the force distribution will affect propeller performance. These pressure changes, as shown in Figures 14 and 15, were at their maximum on the leading edge. This is good for a propeller blade, because at the leading edge, the propeller blade was at its maximum. Therefore, the blade can exert force during operation without failure.

4.7 Vehicle speed and propeller speed relationship

Any change in propeller speed will lead to a thrust change. Therefore, the vehicle speed will also affect propeller speed changes. Another relationship to be discovered, by using CFD, was vehicle speed and propeller speed. Graph in Figure 16 shows the relationship between vehicle speed and propeller speed. To plot the graph, the simulation was run and the thrust produced was recorded. The simulation was run for speeds equal to 0.5, 1, 1.5 and 2.

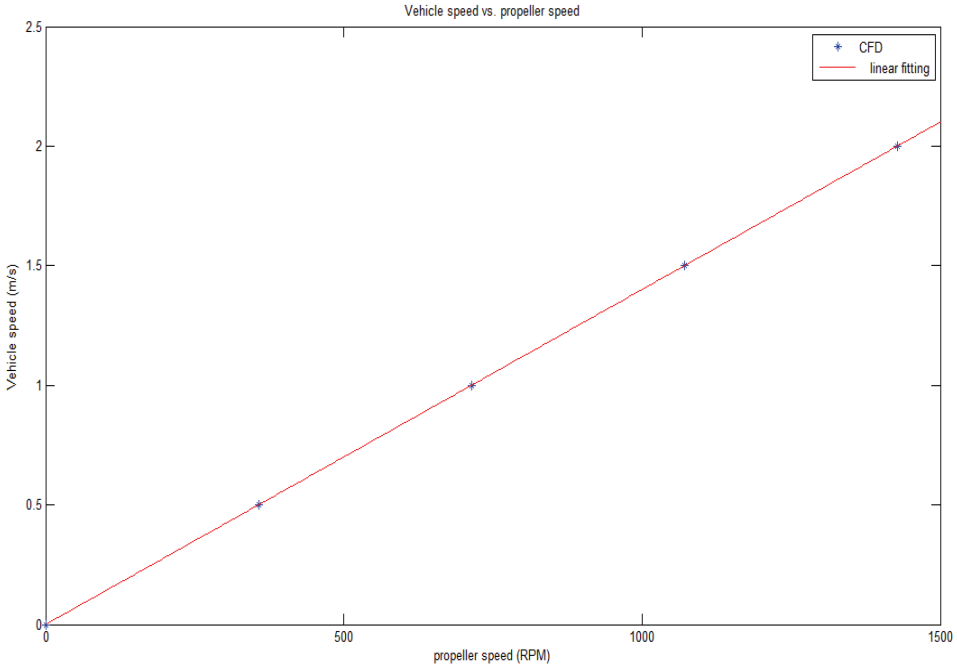

Fig. 16. Relationship between vehicle speed and propeller speed

From the graph in Figure 16, the relationship between speed and rpm can be matched to a linear function. This result was important, because in AUV applications, a precise control system must be developed. By knowing the map between vehicle speed and the propeller speed, a reference value for the control system can be set precisely. This approach will help to save energy consumed in propelling the vehicle. In other words, this method will avoid any waste of energy by randomly guessing the thrust required by the vehicle for a certain speed. This graph was plotted by using the results generated by the CFD simulation. For each speed, there are three levels of rpm to choose from and an approximation was made to find the value of thrust for the vehicles speed.

5. Conclusion

CFD results show the propeller was suitable to be used in AUV because it can give the required thrust. The CFD simulation has been successfully modeling the propeller behavior. In comparison between experiment and simulation for power input, the pattern for the graph was similar. The results show that the CFD can predict the relationship of thrust and torque coefficient for propeller in various advance ratio.

Finally this work has contributed CFD model for AUV propeller. In the literature, only few researchers have simulated AUV propeller. Most of the CFD models were works on marine propellers. Compare with AUV propeller the ship propeller have larger diameter. As mentioned in Carlton (2007) the propeller faces scaling effect when it was directly scale down from bigger size. Thus, to avoid this problem the specific numerical model must be developed in order to get real behavior of the AUV propeller. This research shows that the CFD simulation of AUV propeller was good in agreement with experiment.

In future unsteady CFD simulation of propeller simulation will be done. This study is needed to develop dynamic model of the propeller for precise control system. In this case, the CFD can be applied to support the system identification for nonlinear system such as propeller behavior. Finally, the study can be extended in term of developing the optimum control system that can minimize the energy consumption of AUV.

6. Acknowledgment

We are very grateful to National Oceanographic Directorate (NOD) and Ministry of Science, Technology and Innovation (MOSTI),Malaysia, for providing funding to pursue our research in underwater system technology.

7. References

Benini, E. 2004. Significance of blade element theory in performance prediction of marine propellers. *Ocean Engineering,* 31, 957-974.

Batten, W. M. J., Bahaj, A. S., Molland, A. F. & Chaplin, J. R. 2008. The Prediction of The Hydrodynamic Performance of Marine Current Turbines. *Renewable Energy,* 33, 1085-1096.

Cairns, J., Larnicol, E., Ananthakrishnan, P., Smith, S. & Dunn, S. Year. Design of AUV propeller based on a blade element method. In: *OCEANS '98 Conference Proceedings*, 28 Sep-1 Oct 1998 1998. 672-675 vol.2.

Carlton, J. S. 2007. Propeller design. *Marine Propellers and Propulsion (Second Edition)*. Oxford: Butterworth-Heinemann.

Carlton, J.S., *Propeller design*, in *Marine Propellers and Propulsion (Second Edition)*. 2007, Butterworth-Heinemann: Oxford. p. 435-463.

Celik, F. & Gunner, M. 2007. Energy saving device of stator for marine propellers. *Ocean Engineering,* 34, 850-855.

Chen, J.H. and Y.S. Shih, *Basic design of a series propeller with vibration consideration by genetic algorithm.* Journal of Marine Science and Technology, 2007. 12(3): p. 119-129.

Guo, C. Y., Ma, N. & Yang, C. J. 2009. Numerical Simulation of a Podded Propulsor in Viscous Flow. *Journal of Hydrodynamics,* 21, 71-76.

Ghassemi, H. & Ghadimi, P. 2008. Computational hydrodynamic analysis of the propeller-rudder and the AZIPOD systems. *Ocean Engineering,* 35, 117-130.

Henk Kaarle Versteeg & Weeratunge Malalasekera 2007. *An introduction to computational fluid dynamics,* Harlow,England, Addison Wesley Longman

Hsu, T.H., et al., *An iterative coordinate setup algorithm for airfoil blades inspection.* International Journal of Advanced Manufacturing Technology, 2005. 26(7-8): p. 797-807.

Kerwin, J. E. 2001. "Hydrofoils and Propellers" world wide available at: http://ocw.mit.edu/course/mechanical-engineering/.

Li, D. Q. 2006. Validation of RANS predictions of open water performance of a highly skewed propeller with experiments. *Journal of Hydrodynamics,* 18, 520-528.

Lin, C.-C., Lee, Y.-J. & Hung, C.-S. 2009. Optimization and experiment of composite marine propellers. *Journal of Composite Structure,* 89, 206-215.

Muhamad Husaini, Zahurin Samad, and Mohd Rizal Arshad, CFD Simulation of Cooperative AUV Motion, *Indian Journal of Marine Science* (IJMS), Vol.38(3), pp. *346-351,* September 2009

Neocleous, C. C. & Schizas, C. N. Year. Marine propeller design using artificial neural networks. *In:* Neural Networks, 1999. IJCNN '99. International Joint Conference on, Jul 1999 1999. 3958-3961 vol.6.

Olsen, A.S., *Energy coefficients for a propeller series.* Ocean Engineering, 2004. 31(3-4): p. 401-416.

Phillips, A. B., Turnock, S. R. & FUrlong, M. 2009. Evaluation of manoeuvring coefficients of a self-propelled ship using a blade element momentum propeller model coupled to a Reynolds averaged Navier Stokes flow solver. *Ocean Engineering,* 36, 1217-1225.

Rhee, S. H. & Joshi, S. Year. CFD validation for a marine propeller using an unstructured mesh based RANS method. *In:* Proceedings of the ASME/JSME Joint Fluids Engineering Conference, 2003. 1157-1163.

Rhee, S. H. & Koutsavdis, E. 2005. Two-dimensional simulation of unsteady marine propulsor blade flow using dynamic meshing techniques. *Computers and Fluids,* 34, 1152-1172.

Singhal, A. K., Athavale, M. M., LI, H. & Jiang, Y. 2002. Mathematical basis and validation of the full cavitation model. *Journal of Fluids Engineering, Transactions of the ASME,* 124, 617-624.

Stanway, M.J. and T. Stefanov-Wagner. *Small-diameter ducted contrarotating propulsors for marine robots*. in *OCEANS 2006*. 2006.

Takekoshi, Y., et al., *Study on the design of propeller blade sections using the optimization algorithm.* Journal of Marine Science and Technology, 2005. 10(2): p. 70-81.

Takekoshi, Y., Kawamura, T., Yamaguchi, H., Maeda, M., Ishii, N., Kimura, K., Taketani, T. & Fujii, A. 2005. Study on the design of propeller blade sections using the optimization algorithm. *Journal of Marine Science and Technology,* 10, 70-81.

Takinaci, A.C. and M. Atlar, *Performance assessment of a concept propulsor: the thrust-balanced propeller*. Ocean Engineering, 2002. 29(2): p. 129-149.

Vysohlid, M. & Mahesh, K. 2007. Understanding crashback in marine propellers using an unsteady actuator disk model. In: *Collection of Technical Papers - 45th AIAA Aerospace Sciences Meeting*, 2007. 11133-11140.

Vysohlid, M. and K. Mahesh. *Large Eddy Simulation of crashback in marine propellers*. in *Collection of Technical Papers - 44th AIAA Aerospace Sciences Meeting*. 2006.

Wald, Q. R. 2006. The aerodynamics of propellers. *Progress in Aerospace Sciences,* 42, 85-128.

Yoerger, D. R., Cooke, J. G. & Slotine, J. J. E. (1990) The influence of thruster dynamics on underwater vehicle behavior and their incorporation into control system design. *Oceanic Engineering, IEEE Journal of,* 15, 167-178.

Young, Y. L. & Shen, Y. T. 2007. A numerical tool for the design/analysis of dual-cavitating propellers. *Journal of Fluids Engineering, Transactions of the ASME,* 129, 720-730.